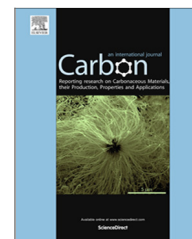


Available at www.sciencedirect.com

ScienceDirect

journal homepage: www.elsevier.com/locate/carbon

Spectral phonon thermal properties in graphene nanoribbons

Zhen-Qiang Ye ^a, Bing-Yang Cao ^{a,*}, Wen-Jun Yao ^a, Tianli Feng ^b, Xiulin Ruan ^{b,*}

^a Key Laboratory for Thermal Science and Power Engineering of Ministry of Education, Department of Engineering Mechanics, Tsinghua University, Beijing 100084, PR China

^b School of Mechanical Engineering and the Birck Nanotechnology Center, Purdue University, West Lafayette, IN 47907-2088, USA

ARTICLE INFO

Article history:

Received 4 March 2015

Accepted 3 June 2015

Available online 10 June 2015

ABSTRACT

This work provides a comprehensive investigation on the spectral phonon properties in graphene nanoribbons (GNRs) by the normal mode decomposition (NMD) method, considering the effects of edge chirality, width, and temperature. We find that the edge chirality has no significant effect on the phonon relaxation time but has a large influence to the phonon group velocity. As a result, the thermal conductivity of around 707 W/(m K) in the 4.26 nm-wide zigzag GNR at room temperature is higher than that of 467 W/(m K) in the armchair GNR with the same width. As the width decreases or the temperature increases, the thermal conductivity reduces significantly due to the decreasing relaxation times. Good agreement is achieved between the thermal conductivities predicted from the Green–Kubo method and the NMD method. We find that optical phonons dominate the thermal transport in the GNRs while the relative contribution of acoustic phonons to the thermal conductivity is only 10.1% and 13% in the zigzag GNR and the armchair GNR, respectively. Interestingly, the ZA mode is found to contribute only 1–5% to the total thermal transport in GNRs, being much lower than that of 30–70% in single layer graphene.

© 2015 Elsevier Ltd. All rights reserved.

1. Introduction

Graphene [1], one of the most important allotropes of carbon, has attracted increasing academic interest due to its unique two-dimensional structure and prominent thermal, mechanical and electrical properties. Graphene is a promising material for thermal management of future nanoelectronic devices due to its high thermal conductivity of 3000–5000 W/(m K) at room temperature [2–6]. It is reported that graphene is one of the hardest nanomaterials [7]. In addition, graphene has an exceptionally high room-temperature carrier mobility, ranging from 15,000 to 27,000 cm²/(Vs) [8–10], which may lead to new applications in carbon-based

electronic and magneto-electronic devices. Graphene nanoribbons (GNRs), whose structures are tunable by changing the edge, length and width, inherit many excellent properties of graphene, and may be used to accomplish a specific goal, such as enhancing the thermoelectric figure of merit [11] and the thermal rectification [12]. From a practical point of view, these outstanding thermal and electronic properties indicate that GNR is a promising material for microelectronic and thermal management in micro-nano devices and circuits.

Since heat dissipation is a crucial issue for the microelectronic industry, the thermal properties of GNRs have attracted much attention. Guo et al. [13] investigated the thermal

* Corresponding authors: Fax: +86 10 62794531 (B.-Y. Cao), +1 7654945721 (X. Ruan).

E-mail addresses: caoby@tsinghua.edu.cn (B.-Y. Cao), ruan@purdue.edu (X. Ruan).

<http://dx.doi.org/10.1016/j.carbon.2015.06.008>

0008-6223/© 2015 Elsevier Ltd. All rights reserved.

conductivity of GNRs with different edge chirality, length, width, and tensile strain using nonequilibrium molecular dynamics (MD) method. Evans et al. [14] studied the effect of edge roughness and hydrogen termination on the thermal conductivity based on the equilibrium MD (EMD). Hu et al. [15] tuned the thermal conductivities of GNRs by edge-passivation and isotope mixture with the aid of MD simulations. In addition, extensive theoretical predictions and experimental measurements have also been carried out. Muñoz et al. [16] studied the dependence of the thermal conductivity of GNRs on the temperature, length and width based on an elastic-shell-based theory. Murali et al. [17] used electrical self-heating to experimentally measure the thermal conductivities of GNRs. Their work showed that GNRs have relatively high and tunable thermal conductivities.

However, to the best of our knowledge, the spectral phonon properties of GNRs have not been studied. Phonons are the main thermal energy carriers for heat conduction in crystals, such as graphene, diamond, etc. The study on the phonon properties of GNRs can provide an insightful understanding of heat conduction in GNRs, and help us to control and tune the heat conduction. Among the phonon properties, phonon relaxation time is an important one, which can be used to estimate the thermal conductivity of a single phonon mode. Raman scattering [18,19] is a common experimental method to measure the relaxation time of a specific mode, but it is only available for limited phonon modes. Aksamija et al. [20] studied phonon–phonon, phonon–isotope, and edge roughness scattering in GNRs by solving the phonon Boltzmann transport equation (BTE) under relaxation time approximation. However, they analyzed the phonons in GNRs based on the dispersion relations of bulk graphene, which are different from those in GNRs especially narrow GNRs. Therefore, it is necessary to study the phonon thermal properties of GNRs based on their own phonon dispersions.

Normal mode decomposition (NMD) is an effective method, which was first introduced by Ladd et al. [21] to analyze the phonon properties of a face-centered cubic crystal with an inverse twelfth-power interatomic potential. Then, it enjoyed great development owing to the efforts from McGaughy and Kaviani [22–24]. To calculate the normal mode of each phonon, the atomic positions from an MD simulation are transformed into the normal mode coordinates. Then, the kinetic and potential energy of each phonon mode are obtained based on it. This method has been successfully used in argon [23], silicon [25], carbon nanotubes (CNTs) [26], graphene [27,28], and others [29]. Therefore, we apply this technique to calculate the spectral phonon properties of GNRs, including dispersion relations, phonon relaxation times, heat capacities, etc. The effect of the width, edge chirality, and temperature on the phonon properties are investigated in detail.

2. Theory and methodology

2.1. Interatomic potential model

The atomic interactions in GNRs are described by the Brenner potential [30], which has been widely applied to hydrocarbon materials [31,32]. Lindsay et al. [33] optimized the parameters

of Brenner potential model and obtained closer thermal conductivity of graphene sheet as compared with experiments. Here, we still used the original parameters, since the general tendencies of the main properties, i.e. dispersion, relaxation time, density of states etc, are not affected by the parameter selection. The Brenner potential is written as

$$\Phi = \sum_i \sum_{j>i} f(r_{ij}) [V_R(r_{ij}) - \bar{b}_{ij} V_A(r_{ij})], \quad (1)$$

in which V_R and V_A are the repulsive and attractive parts of the pairwise binding potential, respectively, and are expressed as

$$V_R(r_{ij}) = \frac{D}{S-1} \exp[-\beta\sqrt{2S}(r_{ij} - R_e)], \quad (2)$$

$$V_A(r_{ij}) = \frac{DS}{S-1} \exp[-\beta\sqrt{2/S}(r_{ij} - R_e)], \quad (3)$$

in which D , S and β are interaction parameters, R_e is the atomic distance at zero potential, and $f(r_{ij})$ is the truncation function that explicitly restricts the interaction within the nearest neighbors. The bond order parameter \bar{b}_{ij} implicitly contains many-body information. Detailed parameters are provided in Ref. [30].

The force constants are derived from the potential energy, which is used in the calculation of phonon dispersion relations. As the precondition of the NMD method, the phonon dispersion relations give important information of lattice vibrations, such as group velocity and density of states (DOS). The force constant matrix [34] is shown in Table 1. It has been proved that interactions of the first four layer interactions are enough to get high accuracy [34]. F_x , F_y and F_z refer to radial, transverse in-plane and transverse out-of-plane, respectively.

We calculate the dispersion relations varying with the chirality. For GNRs, the definition of chirality is exactly the same with CNTs, but the atomic number of each primitive cell is different due to the boundary conditions [35]. For instance, there are 22 atoms in a GNR (5,0) primitive cell, while only 20 atoms in CNT (5,0) primitive cell. In this paper, we will focus on how the edge and width impact the phonon properties, so we investigate the phonons in GNR (5,0), (17,0) and (10,10). The first two are armchair GNRs with different width, and (10,10) belongs to zigzag GNRs with the similar width as (17,0).

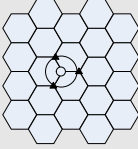
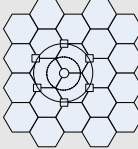
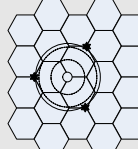
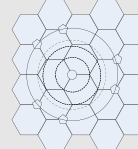
2.2. Lattice dynamics

Phonons are quantized vibrational energy of lattices, so the phonon dispersion relations can be obtained by the lattice dynamics. The atomic motion of the l th atom in the k th cell is described as,

$$m_b \frac{d^2 u_{l,k}}{dt^2} = - \sum_{l',k'}^{s,N_T} F_{(l,k),(l',k')} u_{l',k'}, \quad (4)$$

where m_b is the atomic mass, t is the time, u is the atomic displacement, N_T is the total number of primitive cells, s means the atomic number in each cell, and F is the force constant. The diagonal parameters of the matrix of force constant are shown in Table 1. Eq. (4) has the lattice wave solution,

Table 1 – Force constant parameters for graphene in units of 10^4 dyn/cm.

Layer	1	2	3	4
Parameters				
	$F_x = 36.5$ $F_y = 24.5$ $F_z = 9.82$	$F_x = 8.8$ $F_y = -3.23$ $F_z = -0.4$	$F_x = 3$ $F_y = -5.25$ $F_z = -0.15$	$F_x = -1.92$ $F_y = 2.29$ $F_z = -0.58$

$$u_{l,k} = A_k \exp\{i[q \cdot r_{0(l,k)}] - 2\pi\nu t\}, \quad (5)$$

in which q is the wave vector, A is the amplitude, r_0 refers to the equilibrium position, and ν is the frequency. Then, we substitute Eq. (5) into Eq. (4) and obtain:

$$\omega_{q,j}^2 e_{q,j} = D e_{q,j}, \quad (6)$$

where j means the polarization branch, D is the dynamical matrix, and e is the polarization vector. There are $3 \times s$ branches in the dispersion relations. q and j can determine a unique phonon mode. D is obtained from the force constant matrix as listed in Table 1. The eigenvalues of D are the phonon frequencies, while the eigenvectors are the polarization vectors. By solving Eq. (6), we can get the relations between ν and q , i.e. phonon dispersion relations. We obtained the DOS based on the dispersion relations by dividing the frequency range into many small segments and counting the number of states in each segments. The group velocity is

$$v_g = \frac{\partial \omega}{\partial q}. \quad (7)$$

According to the BTE, the total thermal conductivity of lattice vibrations can be modeled as

$$\lambda = \sum_j \sum_q c_{q,j} v_{g(q,j)}^2 \tau_{q,j}, \quad (8)$$

where c means the heat capacity and τ is the relaxation time.

2.3. Normal mode decomposition

The normal mode Q is expressed as

$$Q_{q,j} = \sqrt{\frac{m_b}{N_T}} \sum_{\alpha} \sum_k^s e_{\alpha(k,q,j)} \left\{ \sum_l^{N_T} u_{\alpha(l,k)} \exp[iq \cdot r_{0(l,k)}] \right\}, \quad (9)$$

where α is the direction in Cartesian coordinate. Our former work [36] has shown that this formalism is equivalent to the version that does not use eigenvectors. The influence of a phonon is reflected in all the atomic vibrations, the vibration of an atom in turn has the contributions from all the phonons. The kinetic and potential energy of a single phonon mode are expressed as

$$E_p = \frac{\omega^2 Q^* Q}{2}, \quad (10.a)$$

$$E_k = \frac{\dot{Q}^* \dot{Q}}{2}, \quad (10.b)$$

$$E = E_k + E_p, \quad (10.c)$$

where E_p , E_k , E are the potential, kinetic and total energy, respectively. The superscript “*” means complex conjugate and “•” refers to derivation. It should be noted that the frequency of the energy is twice that of the normal mode Q theoretically because of the mathematic relationship. The phonon relaxation time is deduced by using the exponential function to fit the heat current autocorrelation function (HCAF) of the total energy,

$$\exp(-t/\tau) = \frac{\langle \delta E(t) \delta E(0) \rangle}{\langle \delta E(0) \delta E(0) \rangle}, \quad (11)$$

in which δ refers to the deviation from the mean value.

The calculation of relaxation times is carried out in EMD simulations. The region is a two-dimensional plane, which has a periodic boundary along the length. We have studied the size effect in our former work [27], and find that 24.6 nm is large enough to eliminate the size effect. Firstly, the system is set up to the designated temperature by the NVT ensemble with the Nose–Hoover thermostat [37] for 200,000 steps. The time step is 0.5 fs. Then, it evolves in a NVE ensemble for the next 5,200,000 steps, in which the first 200,000 steps are used to eliminate the influence of canceling the thermostat, while the next 5,000,000 steps to record the atomic coordinates and velocities. Combining the atomic information with the dispersion relations, the time-varying normal mode of a specific phonon is obtained. Then, the potential and total energy are calculated based on Eq. (10).

3. Results and discussion

3.1. Dispersion relations of graphene nanoribbons

We firstly show the dispersion curves of (5,0), (17,0) and (10,10) in Fig. 1, whose primitive cells have 22, 70 and 41 atoms, with width of 1.23, 4.18 and 4.26 nm, respectively. There are 66, 210 and 123 polarization branches in Fig. 1(a)–(c), respectively, with three acoustic modes, i.e. longitudinal acoustic mode (LA), transverse acoustic mode (TA) and out-of-plane acoustic mode (ZA), and the optical branches. It shows that the phonon frequencies in the two armchair GNRs have similar tendencies. The dispersion relations of (10,10) are different from the two armchair GNRs and generally owning high slopes.

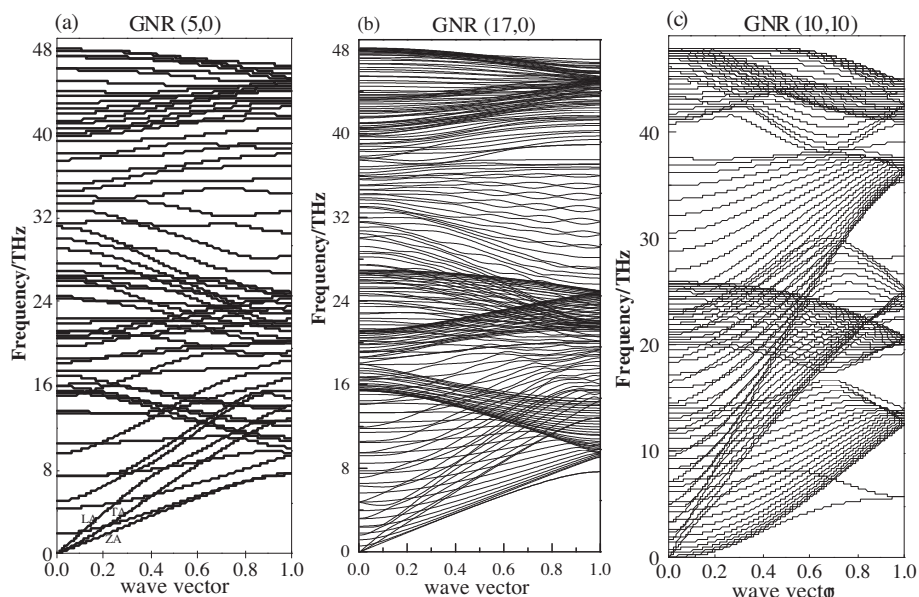


Fig. 1 – Dispersion relations of (a) (5,0), (b) (17,0) and (c) (10,10) GNRs with the normalized wave vector.

The phonon group velocity, which is one of the most important parameters that determine the thermal conductivity, can be extracted from the dispersion relations by differentiation. Whereas the acoustic branches are representative and play a major role in heat conduction, so we only give the group velocities of the three acoustic branches below. Table 2 shows the group velocities at the center of the first Brillouin Zone (BZ). The two armchair GNRs have similar group velocities for all the three acoustic branches, while the zigzag GNR has higher velocities in the LA and TA branches and lower velocities in ZA mode which is only 1.1 km/s. The ZA branch, or flexural mode, has the lowest group velocities in GNRs as well as in graphene [2,29] due to its quadratic dispersion. Fig. 2 gives the acoustic group velocities of the full wave vector space. The ZA branches in the two armchair GNRs almost coincide and higher than that of the zigzag GNR. The two armchair GNRs also own similar group velocities in the TA branches, while in the armchair GNR the group velocity of TA branch is high at the center of BZ and decreases sharply as approaching to the boundary of BZ. It should be noted that the TA branch of the zigzag GNR has a reversal trend, which drops to zero in midway, then goes up. It is due to the derivative of the dispersion is negative in the latter half space, while the group velocities should be changed into absolute value. In general, the ZA branches have the lowest group velocities in most cases, and all of the acoustic branches can reduce to zero at the BZ edge.

Table 2 – Group velocities of the three acoustic branches at the zero point (units: km/s).

	ZA	TA	LA
(5,0)	7.9	9.6	16.7
(17,0)	7.9	9.1	17.4
(10,10)	1.1	12.6	20.1

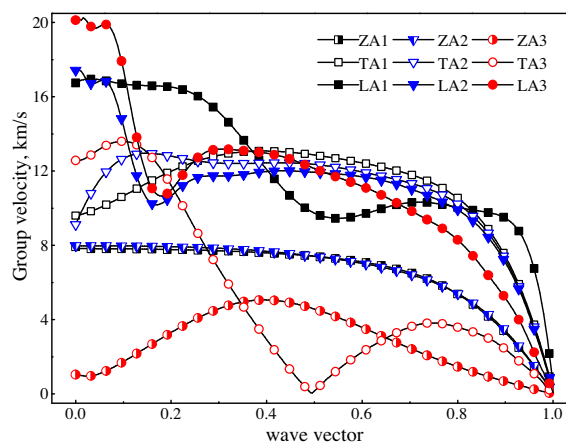


Fig. 2 – Group velocities of LA, TA and ZA branches. Nos. 1–3 refer to GNRs (5,0), (17,0) and (10,10), respectively. (A color version of this figure can be viewed online.)

3.2. Relaxation times of graphene nanoribbons

To clarify the NMD method, Fig. 3 shows the time-varying HCAFs of the potential and total energy. In this case, the phonon frequency is 37.6 THz existing in the armchair GNR. The attenuation of HCAFs of the potential and total energy as shown in Fig. 3(a). Two points should be noted. First, the HCAFs of both potential and total energy have a 95% drop in only a few picoseconds. Second, the potential energy curve declines in an oscillating way, while the total energy curve almost coincides with the outline of the former. In fact, it reflects the transformation between potential and kinetic energies. While the kinetic energy reduces to zero, the potential energy increases to the total energy. Fig. 3(b) shows the partial enlarged view of the potential energy curve. The curve oscillates at a frequency of 72.5 THz, which is nearly twice the phonon frequency 37.6 THz. Fig. 3(c) uses the exponential

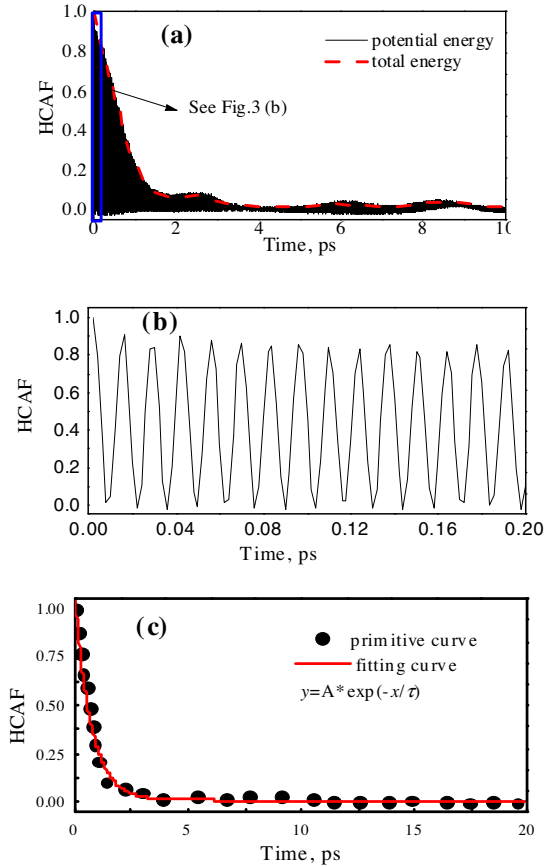


Fig. 3 – (a) HCAFs of the potential and total energy; (b) partial fitting of the potential energy curve; (c) fitting the HCAF of the total energy by the exponential function. (A color version of this figure can be viewed online.)

function to fit the total energy curve. The relaxation time τ is 0.772 ps and the standard error is 0.00976.

Fig. 4 presents the frequency-dependent relaxation times of GNRs (5,0), (17,0) and (10,10) at room temperature in logarithmic scale. An extra case of 1000 K is studied for GNR (10,10) to investigate the effect of the temperature. The phonon relaxation time generally decreases with increasing frequency. From the comparison of (a) and (b), we can see that narrower width gave lower phonon relaxation times. Fig. 4(b) and (c) show a similar order of phonon relaxation time. The relaxations of (10,10) have a significant drop while the temperature increases from 300 K to 1000 K in Fig. 4(c). To explain these phenomena, we introduce the theoretical model of phonon relaxation times [20,38],

$$\frac{1}{\tau} = \frac{1}{\tau_U} + \frac{1}{\tau_B}, \quad (12)$$

in which τ_U and τ_B , respectively, refer to the relaxation times of U-process and boundary scattering. For the U-process scattering, it is expressed as

$$\frac{1}{\tau_U} = \frac{\hbar\gamma^2}{m_b v_g^2 \Theta} \omega^2 T \exp\left(-\frac{\Theta}{3T}\right), \quad (13)$$

and for the boundary scattering, we have

$$\frac{1}{\tau_B} = \frac{v_g}{W} \frac{1-p}{1+p}, \quad (14)$$

here γ means the Grüneisen parameter, Θ is Debye temperature, W is the width and p refers to the specularly parameter of the boundary. The specularly parameter of zigzag GNRs is larger than that of armchair GNRs [20]. The equations show that the reciprocal of the relaxation time is proportional to the square of the frequency if the group velocity hold keeps constant and there is no boundary scattering. So, we add the curve “ $1/\tau \propto \nu^2$ ” in Fig. 4(a)–(c) to compare with the actual trends, which is called “ideal curve” for an illustrative purpose. The comparisons indicate that Fig. 4(a) deviates most from the ideal curve, while in the Fig. 4(b) and (c), the low-frequency parts are relatively close to the ideal curve. The boundary scattering model can well explain the behaviors in Fig. 4(a)–(c). Eq. (14) suggests that the smaller width can lead to the stronger boundary scattering, resulting in the decrease of the relaxation time and the deviation from the ideal curve.

3.3. Heat capacities of graphene nanoribbons

The heat capacity can be obtained from the lattice dynamics analysis,

$$c(\omega) = \frac{\hbar\omega}{V} \frac{\partial f_0}{\partial T} \text{DOS}(\omega), \quad (15a)$$

$$f_0 = \frac{k_B T}{\hbar\omega}, \quad (15b)$$

$$c(\omega) = \frac{k_B}{V} \text{DOS}(\omega), \quad (15c)$$

where f_0 is the Boltzmann distribution. Fig. 5 shows the DOS, which is deduced from the dispersion relations, of GNRs (5,0), (17,0), (10,10) and the single-layer graphene. For the zigzag GNR (10,10), few phonon modes are excited in the range of 25–35 THz, and it has similar peaks with graphene. Generally, the DOS of GNRs are different with that of single-layer graphene.

The frequency-dependent heat capacities of phonons are shown in Fig. 6. For classical mechanics system, heat capacity is temperature-independent and proportional to DOS. The phonons with high heat capacity gather in the high-frequency area. Phonons with frequency around 30 THz and lower than 5 THz have extremely low heat capacities. GNRs (5,0) and (17,0) have lower heat capacities in low-frequency region compared to that of GNR (10,10).

3.4. Thermal conductivities of graphene nanoribbons

In Fig. 7, we show the thermal conductivity accumulation with respect to frequency for the GNRs. At 300 K, the thermal conductivities of GNRs (5,0), (17,0) and (10,10) are respectively 219, 467 and 707 W/(m K), respectively, which are much lower than the thermal conductivity of graphene [3] because of the strong size effect. With the similar widths, zigzag GNRs perform better than armchair GNRs in heat conduction, which agrees with the literature [10–12,20]. In addition, the influence of the edge reflects on the contributions ratio of different phonons. In Fig. 7, the thermal conductivity saturates at after

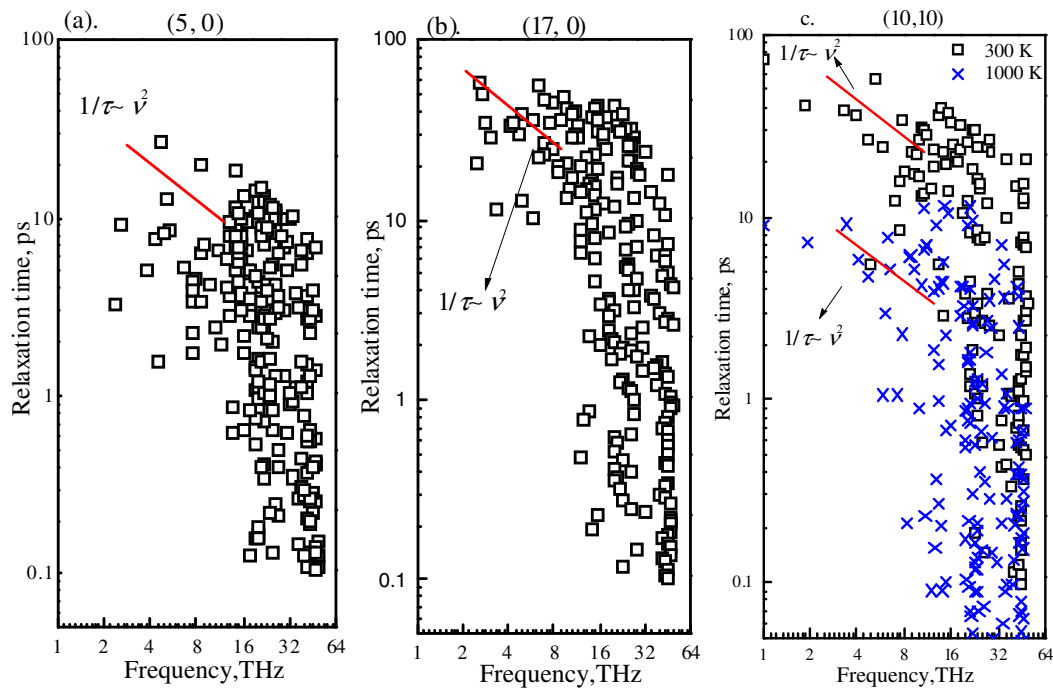


Fig. 4 – Frequency-varying relaxation times of GNR (5,0), (17,0) and (10,10). The diamonds and crosses respectively refer to the NMD results at 300 K and 1000 K. (A color version of this figure can be viewed online.)

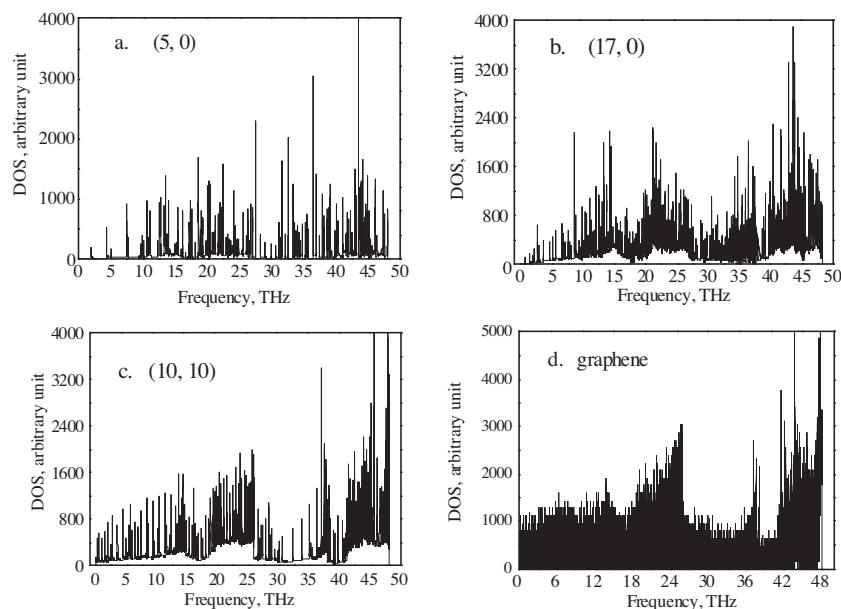


Fig. 5 – DOS of (5,0), (17,0), (10,10) and graphene.

20 THz for GNRs (5,0) and (17,0) and 35 THz for GNR (10,10), indicating the relative contribution of the high-frequency phonons in zigzag GNRs is larger than that in armchair GNRs due to the higher group velocities in high-frequency region. The smaller width leads to the lower thermal conductivity due to the stronger boundary scattering by comparing the thermal conductivity of GNR (5,0) to that of GNR (17,0). As the temperature increases to 1000 K, the thermal

conductivity of GNR (10,10) is reduced to 248 W/(m·K) due to the significant decrease of the relaxation times.

Fig. 8 shows the relative contribution of acoustic phonons to the thermal conductivity. At 300 K, the ratios of ZA, TA, LA and the sum are 4.4%, 10.8%, 11.5% and 26.7% for (5,0); 1.9%, 5.3%, 5.8% and 13% for (17,0); 1.2%, 3.9%, 5.0% and 10.1% for (10,10). The LA phonons contribute the most and ZA modes contribute the least. The LA modes have the most relative

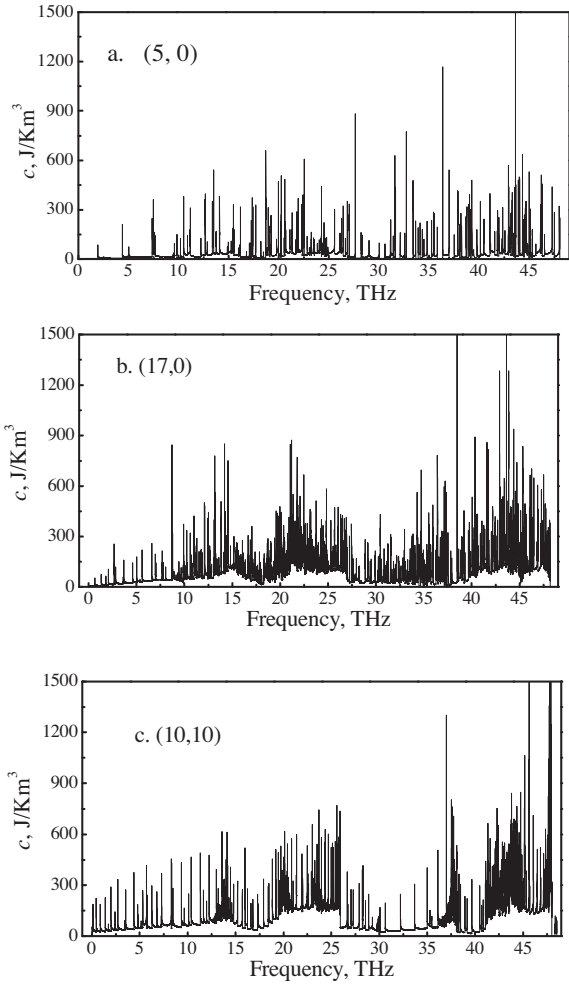


Fig. 6 – Phonon heat capacities of (5,0), (17,0), (10,10).

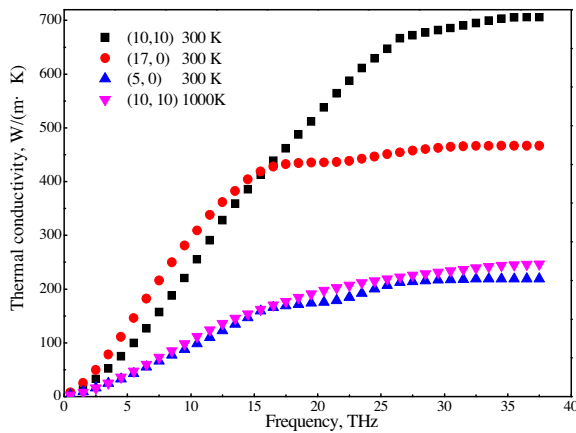


Fig. 7 – Thermal conductivity accumulation with respect to frequency. (A color version of this figure can be viewed online.)

contribution, which are 11.5%, 5.8%, and 5.0% for GNRs (5,0), (17,0) and (10,10) respectively, while the relative contribution of the ZA modes is the least, which are 4.4%, 1.9% and 1.2% respectively. This illustrates a striking contrast to the single

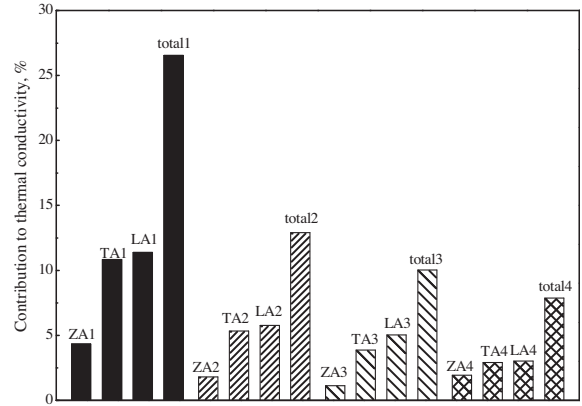


Fig. 8 – Contribution ratio of acoustic phonons to the thermal conductivity. Nos. 1–3 refer to (5,0), (17,0) and (10,10) at 300 K, and No. 4 is for (10,10) at 1000 K.

layer graphene, in which the ZA mode was found to contribute 30–70% to the total thermal conductivity using different approaches [6,29]. The total ratio of acoustic phonons in (10,10) is smaller than in (17,0), and the ratio increases with the decreasing width. The lowest contribution of ZA phonons is due to the group velocity. As shown in Fig. 2, the ZA branches have the lowest group velocities in most region. It has been reported that ZA modes contribute the most in suspended graphene due to the large DOS [6,39,40]. The DOS of ZA phonons in GNRs has no obvious advantages compared to that of other modes, so the contribution ratio of ZA phonons in GNRs is much less than that in graphene. Because of the boundary effect, the primitive cell of GNR has more atoms than that of graphene. As a consequence, many acoustic phonons convert into optical phonons, and the contribution of acoustic phonons significantly decreases. There are 63, 207 and 120 optical branches in (5,0), (17,0) and (10,10) primitive cells, respectively. Hence, it is no surprise that the acoustic phonons in (5,0) have a larger contribution ratio than those in (17,0). Though (10,10) has less optical branches than (17,0), the optical phonons in (10,10) still play more significant role than in (17,0). Because the optical phonons in (10,10) have higher group velocities, the optical phonons still make a relatively high contribution to heat conduction, which is consistent with the results in Fig. 7. At 1000 K, the contribution of the acoustic phonons in (10,10) has a further decline, which drops to 7.9% from 10.1%. With the temperature increasing, the heat capacities of the optical phonons increase much more than those of the acoustic phonons, which enhances the contribution from the optical phonons.

To verify the accuracy of the NMD results, the thermal conductivities of GNRs (17,0) (10,10) at 300 K are calculated by using the Green-Kubo method, which has been widely used in predicting thermal properties [30,41,42]. The Green-Kubo formula is expressed as

$$\lambda = \frac{1}{3VT^2k_B} \int_0^\infty \langle J(t) \cdot J(0) \rangle dt, \quad (16)$$

in which $\langle \rangle$ indicates the ensemble average. $J(t)$ is the heat current flux in the system at t moment, which is calculated based on the formulation in Ref. [43]. The system length

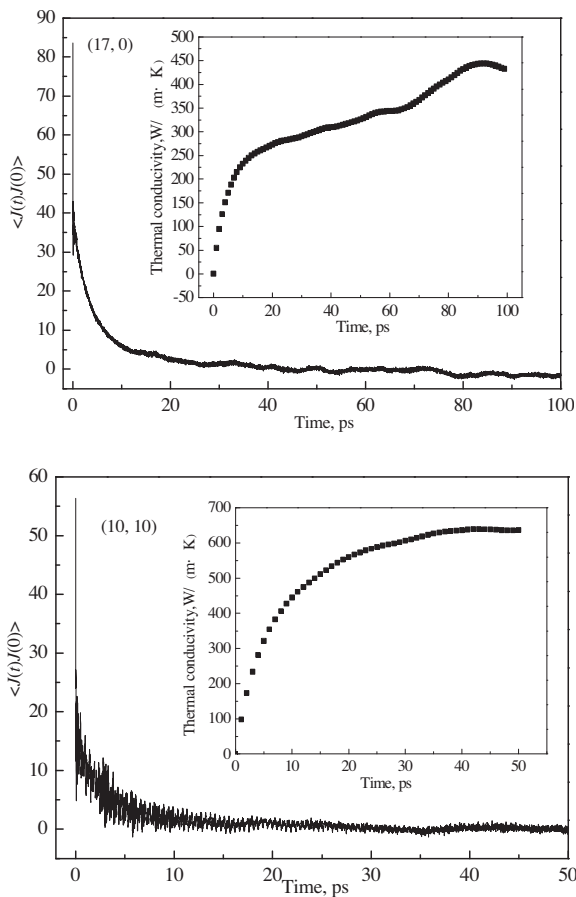


Fig. 9 – $\langle J(t)J(0) \rangle$ and thermal conductivities (insets) of (a) (17,0) and (b) (10,10) calculated by Green–Kubo formula.

24.6 nm can make sure the elimination of the size effect. Actually, this size effect in EMD is different from that caused by the ballistic-diffusive transport [44] in underlying physical mechanism. Fig. 9 shows the attenuation curve of $\langle J(t)J(0) \rangle$ and the integral results of the thermal conductivity. The curves of $\langle J(t)J(0) \rangle$ rapidly reduce to around zero in 20 ps and 10 ps, while their integrations saturate at around 80 ps and 50 ps for GNR (17,0) and (10,10), respectively. It shows that the thermal conductivities of GNRs (17,0) and (10,10) are around 430 W/(m K) and 645 W/(m K) at 300 K, which are close to our NMD results, and slightly higher than the literature values of 400 W/(m K) and 600 W/(m K) [45] using the same method.

4. Conclusion

The spectral phonon thermal properties of GNRs (5,0), (17,0) and (10,10) are investigated at 300 K, while for (10,10) also at 1000 K. The first two are armchair GNRs with different widths, and the last one is a zigzag GNR with a similar width as (17,0), aiming to reveal the effects of edge, width and temperature. First, lattice dynamics is used to calculate the dispersion relations, which are used to deduce the group velocities, DOS and heat capacities. Then, the frequency-dependent relaxation

times are obtained based on the NMD method. Finally, the spectral thermal conductivities are predicted with the above results based on the Boltzmann transport equation.

The dispersion relations of the two armchair GNRs have similar trends, which vary steeply at low frequencies but slowly in the high-frequency region. In contrast, the dispersion relations of (10,10) are different, with relatively high slopes at high frequencies. Therefore, the zigzag GNRs have higher group velocities than the armchair GNRs, especially in the high-frequency region.

The relaxation times of (5,0) are lower than that of the other two GNRs, suggesting that the width has effects on the relaxation times due to strong boundary scattering. Comparing the results of (17,0) and (10,10), it is found that there is no obvious difference, which indicates that the edge chirality has little effect on the relaxation times. The relaxation times of (10,10) have a significant drop at 1000 K, indicating that the high temperature remarkably reduces the relaxation times.

The estimated thermal conductivities are 219, 467 and 707 W/(m K) at 300 K for (5,0), (17,0) and (10,10). Hence, under the same width, the GNRs with the zigzag edge have higher thermal conductivities than those with the armchair edge. Moreover, the relative contribution of acoustic phonons in zigzag GNRs is lower than that in armchair GNRs. In (10,10), the acoustic phonons contribute 10.1% to the thermal conductivity, compared to 13% in (17,0). The thermal conductivity of (5,0) is much less than that of (17,0), which confirms to the influence of the width on the relaxation times. When the temperature increases to 1000 K, the thermal conductivity of (10,10) reduces to 248 W/(m K), and the contribution ratio of the acoustic phonons is down to 7.9%.

Acknowledgment

This work was financially supported by the National Natural Science Foundation of China (No.51322603, 51136001, 51356001), the Program for New Century Excellent Talents in University, Tsinghua National Laboratory for Information Science and Technology, and Science Fund for Creative Research Group (No. 51321002). Tianli Feng and Xiulin Ruan acknowledge partial support from the US National Science Foundation CAREER Award (Grant No. 1150948).

REFERENCES

- [1] Novoselov KS, Geim AK, Morozov SV, Jiang D, Zhang Y, Dubonos S, et al. Electric field effect in atomically thin carbon films. *Science* 2004;306(5696):666–9.
- [2] Nika DL, Ghosh S, Pokatilov EP, Balandin AA. Lattice thermal conductivity of graphene flakes comparison with bulk graphite. *Appl Phys Lett* 2009;94(20):203103-1–3.
- [3] Balandin AA, Ghosh S, Bao W, Calizo I, Teweldebrhan D, Miao F, et al. Superior thermal conductivity of single-layer graphene. *Nano Lett* 2008;8(3):902–7.
- [4] Wei Z, Yang J, Bi K, Chen Y. Mode dependent lattice thermal conductivity of single layer graphene. *J Appl Phys* 2014;116(15):153503-1–11.

- [5] Jauregui L, Yue Y, Sidorov A, Hu J, Yu Q, Lopez G, et al. Thermal transport in graphene nanostructures: experiments and simulations. *ECS Trans* 2010;28(5):73–83.
- [6] Lindsay L, Broido DA, Mingo N. Flexural phonons and thermal transport in graphene. *Phys Rev B* 2010;82(11):115427-1-6.
- [7] Lee C, Wei X, Kysar JW, Hone J. Measurement of the elastic properties and intrinsic strength of monolayer graphene. *Science* 2008;321(5887):385–8.
- [8] Bunch JS, van der Zande AM, Verbridge SS, Frank IW, Tanenbaum DM, Parpia JM, et al. Electromechanical resonators from graphene sheets. *Science* 2007;315(5811):490–3.
- [9] Castro Neto AH, Guinea F, Peres NMR, Novoselov KS, Geim AK. The electronic properties of graphene. *Rev Mod Phys* 2009;81(1):109–61.
- [10] Zhang YB, Tan YW, Stormer HL, Kim P. Experimental observation of the quantum Hall effect and Berry's phase in graphene. *Nature* 2005;438(04235):201–4.
- [11] Nikolic BK, Saha KK, Markussen T, Thygesen KS. First-principles quantum transport modeling of thermoelectricity in single-molecule nanojunctions with graphene nanoribbon electrodes. *J Comput Electron* 2012;11(1):78–92.
- [12] Hu J, Ruan X, Chen YP. Thermal conductivity and thermal rectification in graphene nanoribbons: a molecular dynamics study. *Nano Lett* 2009;9(7):2730–5.
- [13] Guo Z, Zhang D, Gong XG. Thermal conductivity of graphene nanoribbons. *Appl Phys Lett* 2009;95(16):163103-1-3.
- [14] Evans WJ, Hu L, Koblinski P. Thermal conductivity of graphene ribbons from equilibrium molecular dynamics: effect of ribbon width, edge roughness, and hydrogen termination. *Appl Phys Lett* 2010;96(20):203112-1-3.
- [15] Hu J, Schiffl S, Vallabhaneni A, Ruan X, Chen YP. Tuning the thermal conductivity of graphene nanoribbons by edge passivation and isotope engineering: a molecular dynamics study. *Appl Phys Lett* 2010;97(13):133107-1-3.
- [16] Muñoz E, Lu J, Yakobson BI. Ballistic thermal conductance of graphene ribbons. *Nano Lett* 2010;10(5):1652–6.
- [17] Murali R, Yang Y, Brenner K, Beck T, Meindl JD. Breakdown current density of graphene nanoribbons. *Appl Phys Lett* 2009;94(24):243114-1-3.
- [18] Song D, Wang F, Dukovic G, Zheng M, Semke ED, Brus LE, et al. Direct measurement of the lifetime of optical phonons in single-walled carbon nanotubes. *Phys Rev Lett* 2008;100(22):225503-1-4.
- [19] Kang K, Abdula D, Cahill DG, Shim M. Lifetimes of optical phonons in graphene and graphite by time-resolved incoherent anti-stokes Raman scattering. *Phys Rev B* 2010;81(16):165405-1-6.
- [20] Aksamijaa Z, Knezevic I. Lattice thermal conductivity of graphene nanoribbons: anisotropy and edge roughness scattering. *Appl Phys Lett* 2011;98(14):141919-1-3.
- [21] Ladd AJC, Moran B, Hoover WG. Lattice thermal conductivity: a comparison of molecular dynamics and anharmonic lattice dynamics. *Phys Rev B* 1986;34(8):5058–64.
- [22] McGaughey AJH, Kaviani M. Quantitative validation of the Boltzmann transport equation phonon thermal conductivity model under the single-mode relaxation time approximation. *Phys Rev B* 2004;69(9):094303-1–12.
- [23] Kaviani M. *Heat Transfer Physics*. London: Cambridge University Press; 2008.
- [24] Wang Y, Qiu B, McGaughey AJH, Ruan X, Xu X. Mode-wise thermal conductivity of bismuth telluride. *J Heat Trans* 2013;135(9):091102-1-6.
- [25] Henry AS, Chen G. Spectral phonon transport properties of silicon based on molecular dynamics simulations and lattice dynamics. *J Comput Theor Nanosci* 2008;5(2):141–52.
- [26] Thomas JA, Turney EJ, Iutzi RM, Amon CH, McGaughey AJH. Predicting phonon dispersion relations and lifetimes from the spectral energy density. *Phys Rev B* 2010;81(8):081411-1–4.
- [27] Ye ZQ, Cao BY, Guo ZY. Study on thermal characteristics of phonons in graphene. *Acta Phys Sin* 2014;63(15):154704-1–5 (In Chinese).
- [28] Feng T, Ruan X, Ye ZQ, Cao BY. Spectral phonon mean free path and thermal conductivity accumulation in defected graphene: The effects of defect type and concentration. *Phys Rev B* 2015;91(22):224301-1–12.
- [29] Feng T, Ruan X. Prediction of spectral phonon mean free path and thermal conductivity with applications to thermoelectrics and thermal management: a review. *J Nanomater* 2014;2014(2014):206370-1–25.
- [30] Brenner DW. Empirical potential for hydrocarbons for use in simulating the chemical vapor deposition of diamond films. *Phys Rev B* 1990;42(15):9458–71.
- [31] Ye ZQ, Cao BY, Guo ZY. High and anisotropic thermal conductivity of body-centered tetragonal C4 calculated using molecular dynamics. *Carbon* 2014;66(6):567–75.
- [32] Tang C, Guo WL, Chen CF. Structural and mechanical properties of partially unzipped carbon nanotubes. *Phys Rev B* 2011;83(7):075410-1–6.
- [33] Lindsay L, Broido DA. Optimized Tersoff and Brenner empirical potential parameters for lattice dynamics and phonon thermal transport in carbon nanotubes and graphene. *Phys Rev B* 2010;81(20):205441-1–6.
- [34] Saito R, Dresselhaus G, Dresselhaus MS. *Physical Properties of Carbon Nanotubes*. London: Imperial College Press; 1998.
- [35] Jiao L, Zhang L, Wang X, Diankov G, Dai H. Narrow graphene nanoribbons from carbon nanotubes. *Nature* 2009;458:877–80.
- [36] Feng T, Qiu B, Ruan X. Anharmonicity and necessity of phonon eigenvectors in the phonon normal mode analysis. *J Appl Phys* 2015;117(19):195102-1–5.
- [37] Hunenberger PH. Thermostat algorithms for molecular dynamics simulations. *Adv Polym Sci* 2005;173:105–49.
- [38] Morelli DT, Heremans JP, Slack GA. Estimation of the isotope effect on the lattice thermal conductivity of group IV and group III–V semiconductors. *Phys Rev B* 2002;66(19):195304-1–9.
- [39] Seol JH, Jo I, Moore AL, Lindsay L, Aitken ZH, Pettes MT, et al. Two-dimensional phonon transport in supported graphene. *Science* 2010;328(5975):213–6.
- [40] Lindsay L, Li W, Carrete J, Mingo N, Broido DA, Reinecke TL. Phonon thermal transport in strained and unstrained graphene from first principles. *Phys Rev B* 2014;89(15):155426-1–7.
- [41] Berber S, Kwon YK, Tománek D. Unusually high thermal conductivity of carbon nanotubes. *Phys Rev Lett* 2000;84(20):4613–6.
- [42] Che JW, Çağın T, Deng WQ, Goddard WA. Thermal conductivity of diamond and related materials from molecular dynamics simulations. *J Chem Phys* 2000;113(16):6888–900.
- [43] Khadem MH, Wemhoff AP. Comparison of Green-Kubo and NEMD heat flux formulations for thermal conductivity prediction using the Tersoff potential. *Comput Mater Sci* 2013;69:428–34.
- [44] Hua YC, Cao BY. Phonon ballistic-diffusive heat conduction in silicon nanofilms by Monte Carlo simulations. *Int J Heat Mass Transf* 2014;78:755–9.
- [45] Wang Y, Qiu B, Ruan XL. Edge effect on thermal transport in graphene nanoribbons: a phonon localization mechanism beyond edge roughness scattering. *Appl Phys Lett* 2012;101(1):013101-1–4.